INTERNATIONAL JOURNAL OF CLIMATOLOGY
Int. J. Climatol. (2013)
Published online in Wiley Online Library
(wileyonlinelibrary.com) DOI: 10.1002/joc.3692

RMetS
Royal Meteorological Society

Methods for uncertainty assessment of climate models and model predictions over East Asia

Ki-Young Heo,[a] Kyung-Ja Ha,[b]* Kyung-Sook Yun,[b] Sun-Seon Lee,[b] Hyung-Jin Kim[c] and Bin Wang[d]

[a] *Climate Disaster Research Center, Korea Institute of Ocean Science & Technology, Ansan, South Korea*
[b] *Division of Earth Environmental System, Pusan National University, Busan, South Korea*
[c] *Research Institute for Global Change (RIGC), Japan Agency for Marine-Earth Science and Technology (JAMSTEC), Yokosuka, Japan*
[d] *Department of Meteorology and International Pacific Research Center, University of Hawaii, Honolulu, HI, USA*

ABSTRACT: Model performance and uncertainty have been assessed using simulations of the climate in the 20th century based on the 21 models of the Intergovernmental Panel on Climate Change's Fourth Assessment Report (IPCC AR4) and NCEP/NCAR reanalysis data. To evaluate the fidelity and reliability of the simulations of East Asian climate change, the following approaches are compared to assess the uncertainty of East Asian monsoon and climate projection in conjunction with global warming: Taylor diagrams using correlation and standard deviation of model results over East Asia (100°E–150°E, 20°N–45°N), signal-to-noise ratio (SNR), and principal-mode comparison identified by empirical orthogonal function (EOF) analysis. On the basis of the Taylor diagram and SNR results, good performance models with statistically high fidelity produce higher values of warming over East Asia and an enhancement of the northwest–southeast temperature gradient between the land and ocean. This enhanced temperature gradient may strengthen the East Asian summer monsoon flow, resulting in a greater increase in precipitation along the East Asian summer rain band on the continental side of East Asia. However, the good performance models as determined by the principal-mode comparison produce lower values of warming over the East Asia region during winter; these values are clearly different from the corresponding values obtained from the Taylor diagram and SNR approaches. These results suggest that the models that give priority to the signal associated with the first leading mode of EOF or the principal mode may predict less warming than other models. The models that predict an El Niño-like state in response to greenhouse warming produce less warming over East Asia, corresponding to the results of the principal-mode comparison.

KEY WORDS uncertainty assessment; fidelity; IPCC AR4; model performance; East Asian climate change

Received 1 June 2012; Revised 11 November 2012; Accepted 18 February 2013

1. Introduction

Climate models play important roles in the study of the dynamics of the earth's climate system by simulating present and past climates and predicting future climate changes in response to an increase in CO_2 levels (Reichler and Kim, 2008). A number of modelling centres around the world have performed climate simulations and projections to better understand climate change, particularly in support of the Fourth Assessment Report of the Intergovernmental Panel on Climate Change (IPCC AR4). To date, about 22 coupled global climate models (CGCMs) have been included in a coordinated model intercomparison targeted by the IPCC AR4 to assess future climate changes and anthropogenic contributions to global warming. Although there is a general consensus that climate models provide quantitatively credible estimates of future climate change, significant intermodel variability is still found in the uncertainty associated with detecting the footprint of anthropogenic warming on regional to global scales, likely as a result of widely differing model configurations and physical parameterizations (IPCC, 2007). IPCC (2007) also pointed out that significant uncertainties are associated with the representation of clouds and the resulting cloud responses to climate change, leading to large discrepancies in future climate projections between models, particularly on a regional scale (Schaller *et al*., 2011).

Several statistical approaches have been proposed to extract the potential predictability of climate models on the bases of their uncertainty. Relative entropy, for example, has been considered frequently in previous studies (Kullback, 1959; Cover and Thomas, 1991; Kleeman, 2002; DelSole, 2004; Tippett *et al*., 2004; Delsole and Tippett, 2007). Recently, Shukla *et al*. (2006) evaluated the relative entropy of surface air temperature from 100-year simulations. They found that climate models exhibiting higher fidelity in simulating the present

* Correspondence to: K. -J. Ha, Division of Earth Environmental System, Pusan National University, Busan, Korea. E-mail: kjha@pusan.ac.kr

climate produce more pronounced global warming. Reichler and Kim (2008) evaluated model performance using the model performance index, which is defined as the aggregate of errors in the simulation of the observed climatological mean states of climate variables; this includes eight variables in the atmosphere and six variables in the ocean. Taylor (2001) and Boer and Lambert (2001) characterized the reliability of models with the aid of conventional statistical moments including root mean square error (RMSE), correlation, and variance ratio (standard deviation). Using similar parameters, Gleckler *et al*. (2008) analysed a number of climate variables, including 18 atmospheric variables and 5 oceanic variables, simulated by 22 climate models. They showed that model performance is sensitive to observational uncertainty, spatial scale, and the domain considered (e.g. tropics *vs* extratropics).

The signal-to-noise ratio (SNR) is another statistical measure used frequently to assess model performance and has the merit of being able to identify the robustness of predicted trend signals. Considerable work has been conducted with the SNR to calculate the potential predictability of climate on seasonal to interannual and decadal timescales (Zwiers and von Storch, 2004, and references cited therein). Yeh and Kirtman (2006) utilized the SNR to demonstrate the characteristics of the signal *versus* the noise for sea surface temperature (SST) variability. Labraga (2005) assessed variations in the simulation skill of a climate model using statistical measures and SNR distribution. Tang *et al*. (2008) used the SNR to define the potential predictability of the ensemble climate predictions of the El Niño–Southern Oscillation (ENSO) and the Arctic Oscillation. In addition to the abovementioned statistical approaches, the empirical orthogonal function (EOF) yields information about the dominant modes of variability, from which a more balanced view can be provided of the significance of changes in model predictions across multiple fields, seasons, and regions (Mu *et al*., 2004).

Shukla *et al*. (2006) argued that climate models producing better simulations of the present climate should be considered to be more credible in projecting future climate change. Furthermore, a multimodel ensemble usually yields better performance than any single model (Lambert and Boer, 2001; Gleckler *et al*., 2008). Thus, it is plausible to argue that a group of climate models with small uncertainty should be more reliable in projecting future climate change. Moreover, the evaluation of climate model performance may depend upon the choice of methods and the variables examined. Despite the importance of uncertainty assessment in future climate prediction using CGCMs, there is a lack of research evaluating the fidelity and reliability of the simulations of East Asian climate change.

Here, our main purpose is to evaluate the performance of current climate models using various approaches and to determine a good model (GM) group with small uncertainty relevant to the projection of future climate change over East Asia. To this end, the fidelity and reliability of the present climate simulation must be assessed before future climate prediction. We first investigate the reality of present climate simulations by comparing them with observations using the Taylor diagram (Taylor, 2001). Second, the SNR is calculated from present climate simulations to examine the potential predictability. Finally, we assess the realism of the simulated leading EOF modes to evaluate model performance from a dynamical point of view. Emphasis is placed on addressing the differing (and/or common) aspects of future climate changes arising from the choice of GMs, with a particular focus on the contrast between the statistical and dynamical perspectives. The assessment of uncertainty in the East Asian climate simulations will provide valuable information for future climate change over the region of interest, especially for the application of statistical or dynamical downscaling.

The next section briefly describes the data and models used in this study. Section 3 introduces several methodologies designed to measure the uncertainty, performance, and predictability of CGCMs. Section 4 presents the results of uncertainty assessments and ensemble predictions of various GMs, which are determined by the three different methods. Finally, a summary and discussion are presented in Section 5.

2. Models and validation datasets

The evaluation of model performance is based on the fidelity of the 20th century coupled climate model (20C3M) simulations from 21 IPCC AR4 CGCMs over a period covering 50 years from 1950 to 1999 (the data are defined at the URL http://www-pcmdi.llnl.gov/ipcc/standard_output.html). Table I summarizes the models (for model descriptions, see also the URL http://www.pcmdi.llnl.gov/ipcc/model_documentation/ipcc_model_documentation.php). Monthly mean data including air temperature at 925 hPa, precipitation, and skin temperature are used.

Over East Asia, the East Asian monsoon is characterized by a distinct seasonal reversal of monsoon flow driven by temperature differences between the Pacific Ocean and the East Asian continent. Because of this distinct difference, the annual cycle of the East Asian monsoon can be divided into warm, wet summer and cold, dry winter monsoons (Ha *et al*., 2012). At this point, we focus on the uncertainty assessment for changes associated with the East Asian monsoon, such as those of winter (January to March, JFM) air temperature and summer (June to August, JJA) precipitation. We used JFM as the northern winter (late winter) for convenience of calculation, which we deem acceptable because a linear trend in JFM during the 50 years from 1950 to 1999 (present) is similar to that in DJF over the East Asia region (not shown). For fair comparison, the model outputs are remapped onto a uniform grid system of $2.5^\circ \times 2.5^\circ$ by conducting bilinear interpolation. The future climate changes are derived from the difference between the 20C3M simulations and

Table I. A list and description of models used in this study.

IPCC ID	Label in figures and tables	Resolution model top	References
CGCM3.1-T63	CGCM3.1(T63)	T63 × L32, 2.2 hPa	McFarlane *et al*. (2005), Scinocca *et al*. (2008)
CGCM3.1-T47	CGCM3.1(T47)	T47 × L32, 2.2 hPa	McFarlane *et al*. (2005), Scinocca *et al*. (2008)
CNRM-CM3	CNRM-CM3	T63 × L45, 0.05 hPa	Salas-Mélia *et al*. (2005)
CSIRO Mk3.0	CSIRO-MK3.0	T63 × L18, 4 hPa	Gordon *et al*. (2002)
CSIRO Mk3.5	CSIRO-MK3.5	T63 × L18, 4 hPa	Gordon *et al*. (2002)
GFDL-CM2.0	GFDL-CM2.0	144 × 90 × L24, 3 hPa	Delworth *et al*. (2006)
GFDL-CM2.1	GFDL-CM2.1	144 × 90 × L24, 3 hPa	Delworth *et al*. (2006)
GISS-AOM	GISS-AOM	90 × 60 × L12	Lucarini and Russell (2002)
GISS Model E-H	GISS-EH	72 × 46 × L20, 0.1 hPa	Schmidt *et al*. (2006)
GISS Model E-R	GISS-ER	72 × 46 × L20, 0.1 hPa	Schmidt *et al*. (2006)
FGOALS-g1.0 (IAP)	IAP-FGOALS1.0	64 × 32 × L26, 2 hPa	Yu *et al*. (2004)
IPSL-CM4	IPSL-CM4	96 × 72 × L19	Marti *et al*. (2005)
MIROC3.2-hires	MIROC3.2(hires)	T106 × L56	K-1 model developers (2004)
MIROC3.2-medres	MIROC3.2(medres)	T42 × L20, 30 km	K-1 model developers (2004)
INM-CM3.0	INMCM3.0	72 × 45 × L21	Diansky and Volodin (2002)
ECHAM5/MPI-OM	ECHAM5/MPI-OM	T63 × L31, 10 hPa	Jungclaus *et al*. (2006)
MRI-CGCM2.3.2	MRI-CGCM2.3.2	T42 × L30, 0.4 hPa	Yukimoto and Noda (2002)
NCAR CCSM3	NCAR-CCSM3.0	T83 × L26, 2.2 hPa	Collins *et al*. (2006)
NCAR PCM1	NCAR-PCM1	T42 × L26, 2.2 hPa	Washington *et al*. (2000)
Met Office HadCM3	ukMO-HadCM3	T83 × L18, 4 hPa	Gordon *et al*. (2000)
Met Office HadGEM1	ukMO-HadGEM1	T63 × L18, 4 hPa	Johns *et al*. (2004)

the Special Report on Emissions Scenarios' (SRES) A1B simulations for the period 2050–2099.

To validate the 20C3M simulations, we use the Climate Prediction Center Merged Analysis of Precipitation (CMAP) rainfall data (Xie and Arkin, 1997), the National Centers for Environmental Prediction–National Center for Atmospheric Research reanalysis dataset (NCEP-1; Kalnay *et al*., 1996), and the Hadley Centre Sea Ice and Sea Surface Temperature (HadISST) dataset (Rayner *et al*., 2003) acquired by the British Atmospheric Data Centre.

3. Approaches for uncertainty assessment

Sources of uncertainty in future climate change include uncertainties due to the choice of CGCMs, climate variability, variability within and between models, future natural variability, and systematic discrepancy between models and future reality. In this study, we consider the uncertainties due to choice of CGCMs, climate variability, and variability within and between models. For the uncertainty assessment, we use methods including relative entropy, Taylor diagrams, SNR, and principal-mode comparison. To assess the uncertainty due to the choice of CGCMs, we determine the GM and poor model (PM) groups and evaluate their multimodel ensemble mean (MMEM) change. Relative entropy, which can be interpreted as a measure of the difficulty of discriminating between forecasts and climatological distributions, depends on the SNR of a single forecast distribution (Delsole, 2004; Delsole and Tippet, 2007). The reliability and predictability of dominant features over the East Asia region (i.e. those produced by models) can be assessed by EOF analysis, which can be conducted for different seasons (e.g. winter only or summer only). Because the EOF analysis can also be conducted for observational data, the characteristics of model error can be analysed and the reliability of dominant modes of model climatology can be evaluated. The similarity of the dominant signal and noise patterns can be measured by the spatial correlation between EOF patterns of model output and those of observations (Santer *et al*., 1994).

3.1. Relative entropy

Relative entropy is a measure of the difference between two probability distributions and can capture a statistical difference between observations and model simulations (Kleeman, 2002; Shukla *et al*., 2006); furthermore, it is an objective measure of skill, either in the perfect model scenario or when the goal is to quantify model errors and uncertainties (Giannakis and Majda, 2012). Small values of relative entropy indicate that a given model's distribution is close to that of the observations (Shukla *et al*., 2006). Relative entropy, which can be decomposed into dispersion and signal components, evaluates both the predictability of the spread (dispersion) and the evolution of the mean (signal) of the model prediction. In this study, we use a simplified formula that is focused on the interannual variability of a given variable (see Appendix for details).

3.2. Taylor diagram

The Taylor diagram provides a statistical summary of how well the modelled patterns match the observed patterns in terms of correlation, centred RMSE, and variance. The diagram can be visualized as a series of points on a polar plot. The azimuth angle, φ, pertaining to each point is such that $\cos(\varphi)$ is equal to the correlation coefficient between the modelled and observed data. Radial distance from the origin in the Taylor diagram represents

the ratio of the standard deviation of the simulation to that of the observation, and the pattern correlation between two fields is given by the azimuthal position. The distance from the reference point (observations) is a measure of the centred RMSE. Therefore, an ideal model (being in full agreement with observations) is marked by the reference point (0.1) with coordinates $\varphi = 0$ and radius $= 1$; this means the correlation coefficient is equal to 1, and the modelled and measured variations have the same amplitude.

3.3. Signal-to-noise ratio

The SNR is a measure of a desired signal relative to the background noise. A high SNR implies that the signal is significantly larger than the noise, indicating that the simulated result is robust. Conversely, a low SNR makes any signal difficult to detect. We calculate the SNR as a function of correlation and average noise between two time series, following the method of Trenberth *et al*. (1992) (see the Appendix).

3.4. Principal-mode comparison

The first leading modes of variability over East Asia (100°E–150°E, 20°N–45°N) are extracted from the 20C3M simulations and the observations based on the EOF analysis, which is performed on the linearly detrended temperature anomaly fields. Then, the correlations between the model outputs and observations for the first leading mode (EOF1) of the covariance matrix and its associated principal component (PC1) are used to measure quantitatively the performance of the CGCMs.

In addition, to evaluate the impact of SST variability over the tropical Pacific (10°S–10°N, 120°E–80°W) on climate change over East Asia, we adopt an approach similar to that suggested by Guilyardi *et al*. (2009) and compute a change in the tropical Pacific mean state from a CGCM. The change in the tropical Pacific mean state is defined as a spatial correlation between the EOF1 pattern derived from the 20C3M SST and a linear trend pattern obtained from the SRESA1B SST. A strong correlation between model output and observations of the change in the tropical Pacific mean state suggests that the model predicts El Niño-like warming over the tropical Pacific for the future climate.

4. Uncertainty assessment

4.1. Characteristics of uncertainty in the 20C3M simulations

Prior to the assessment of uncertainty, it is important to investigate the effects of intermodel differences on projections of future climate change. To this end, the range of uncertainty is defined for each grid box as a maximum minus minimum of the future projection obtained from the suite of 21 CGCMs for the period 2079–2099; then, the ratio of this range to MMEM change is calculated. A high range-to-mean ratio (i.e. >1) indicates that the intermodel spread in the SRESA1B simulations surpasses the MMEM change between the 20C3M and SRESA1B simulations.

Figure 1 illustrates the MMEM change and range-to-mean ratio for JFM 925-hPa temperature and JJA precipitation over East Asia. Higher warming is projected primarily over continental regions, particularly in northern China and Korea, where relatively small range-to-mean ratios are evident. The increase in temperature is greater in winter than in summer and the interannual variability is also projected to be stronger in winter than in summer (not shown). The MMEM predicts a 3.2 °C (2.6 °C) temperature increase over the Korean Peninsula in winter (summer) with a range of 0.8 °C (1.1 °C). The MMEM change for the JFM 925-hPa temperature indicates greater warming over the land than the ocean, which enhances the northwest–southeast temperature gradient (Figure 1(a)). Higher intermodel ranges are found over the ocean, especially to the northeast and south of Japan (Figure 1(b)). These results show that, over East Asia, the intermodel difference in regional climate projection is larger over the ocean than over land. An increase in JJA precipitation is found over the East Asian summer monsoon (EASM) region, including Korea, Japan, and China (Figure 1(c)). The range-to-mean ratio of JJA precipitation is significantly higher than that of JFM 925-hPa temperature, suggesting that the complicated rainfall systems hamper reliable prediction. Nevertheless, the ratio along the rain band to the east of 120°E between 30°N and 35°N is relatively low, suggesting that the MMEM is useful in prediction of the change in JJA precipitation in the major regions affected by the EASM. A large range in predicted maximum and minimum indicates large climate variability among climate models; it also indicates differences in climate model responses to changes in climate forcing and future changes in forcing. Therefore, to ensure credible assessment of projections of regional climate change over East Asia, it is important to choose models that exhibit less uncertainty over the region. In this study, we perform an uncertainty assessment using primarily JFM 925-hPa temperature because of the large range-to-mean ratio of JJA precipitation.

4.2. Results from relative entropy

The changes in JFM 925-hPa temperature, derived from the 21 CGCMs over a period of 25 years (2075–2099), are plotted against the relative entropy in Figure 2. Here, the error bars represent the uncertainty (in other words, standard deviation) for the corresponding period. Note that three models (GFDL-CM2.0, GFDL-CM2.1, and IPSL-CM4) describing relative entropy larger than 25 are excluded. The larger relative entropy implies poor performance for present climate simulation, which corresponds to a larger difference between the averages of simulated and observed air temperatures. The larger difference is related to a larger signal component of the relative entropy presented in Equation (A1). Good performance models with small relative entropy tend to predict a significant increase in JFM 925-hPa temperature

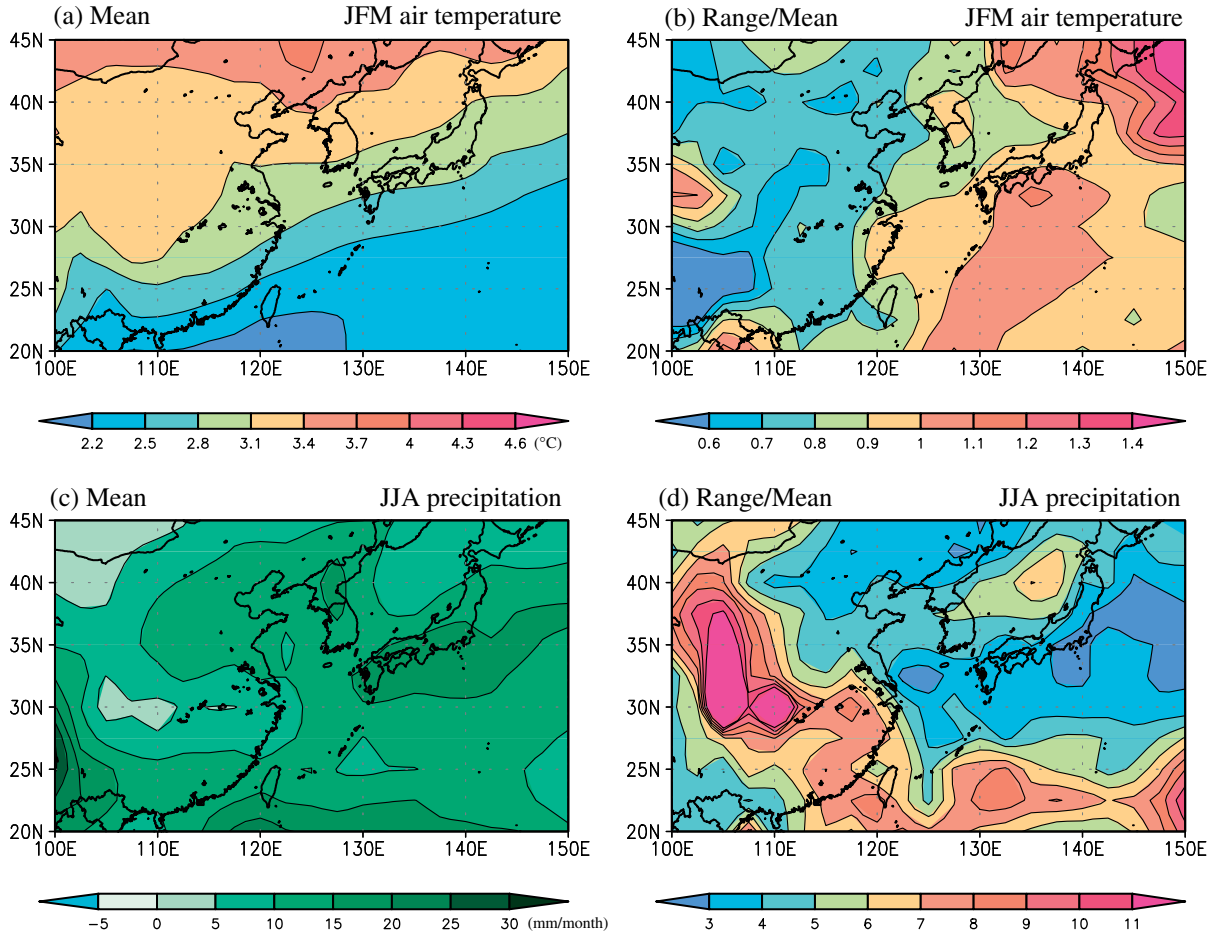

Figure 1. (a) Mean and (b) range-to-mean ratio of JFM air temperature from 21 IPCC AR4 models over East Asia (100°E–150°E, 20°N–45°N). (c) and (d) are the same as (a) and (b), respectively, but for JJA precipitation. This figure is available in colour online at wileyonlinelibrary.com/journal/joc

over East Asia (100°E–150°E, 20°N–45°N), which is consistent with the result of Shukla *et al*. (2006). The correlation coefficient between sensitivity (i.e. temperature increase) and fidelity (i.e. relative entropy) is −0.49 with confidence level higher than 95%.

4.3. Results from the Taylor diagram

Figure 3 displays the normalized standard deviation and correlation coefficient (with reference to the observations) for JFM 925-hPa air temperature and JJA precipitation derived from the 20C3M simulations. The spatial patterns of JFM 925-hPa temperature are reproduced more accurately than those of JJA precipitation, with the latter having a relatively high RMSE (Figure 3). On the basis of these results, GMs are identified for JJA precipitation and JFM 925-hPa temperature; these are listed in Tables II and III, respectively. On the basis of the results shown in the Taylor diagram, five GMs for the variables are determined by concentric analysis with respect to the ideal model point (0.1). Thereafter, a grand GM for the Taylor diagram is defined as a collection of five models that are commonly identified as GMs for both variables (Table IV). Meanwhile, the PM for the Taylor diagram is composed of the models that perform poorly for both variables. The resultant GM and PM for the Taylor diagram are presented in Table IV.

Over East Asia, the GM for the Taylor diagram predicts a larger JFM warming (with a maximum of 4.6 °C over northern China) than the PM (with a maximum of 4.0 °C north of the Korean Peninsula); this is illustrated by Figure 4(a) and (b) and the MMEM shown in Figure 1(a), and is consistent with the result from the relative entropy (Figure 2). The GM predicts an enhanced northwest–southeast temperature gradient between the land and ocean, corresponding to the MMEM. The intensified temperature gradient also occurs in JJA (Figure 4(c)). Owing to this change in land–ocean temperature gradients, anomalous ascending and descending motions occur over the northern land and southern ocean areas, respectively, with strengthened EASM flow. As a result, the strengthened EASM flow transports more moisture from the East China Sea to Korea and Japan, inducing a 15–20 mm increase in precipitation over Korea and Japan during JJA (Figure 4(e)), which is similar to the result of Bueh *et al*. (2003). In contrast, JFM 925-hPa temperature in the PM ensemble mean shows stronger warming over the ocean, where larger range-to-mean ratios are evident (as shown

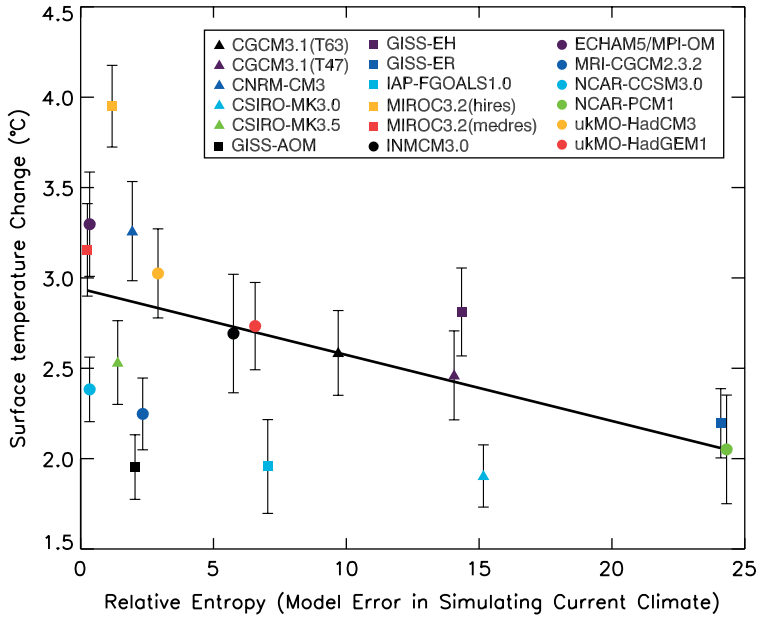

Figure 2. Model sensitivity – i.e., change in surface air temperature during JFM over East Asia (100°E–150°E, 20°N–45°N) – against relative entropy for 15 IPCC AR4 models. Estimates of the uncertainty in the surface temperature change are shown as vertical error bars. The line is a least-squares fit to the values. This figure is available in colour online at wileyonlinelibrary.com/journal/joc

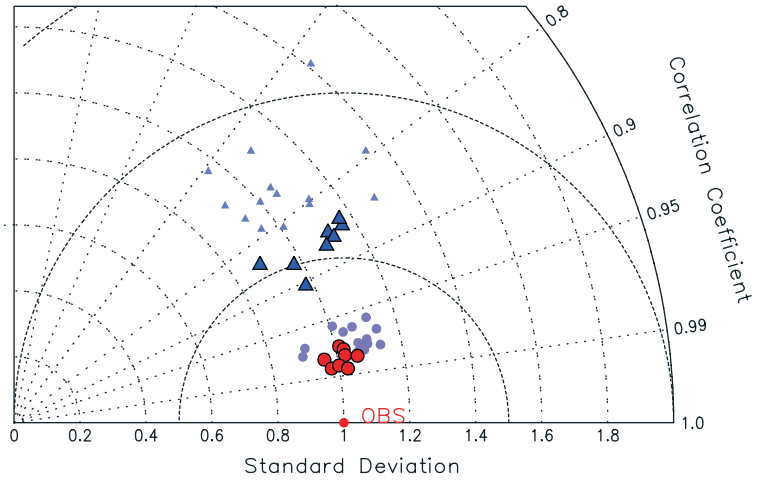

Figure 3. Multivariable Taylor diagrams of the 21 IPCC AR4 GCMs for climatology over East Asia (100°E–150°E, 20°N–45°N), including JFM 925-hPa air temperature (circle) and JJA precipitation (triangle). Large triangles and circles represent good performance models for each variable. The good performance models for JFM 925-hPa air temperature and JJA precipitation are presented in Tables II and III. This figure is available in colour online at wileyonlinelibrary.com/journal/joc

in Figure 1(b)), and a strong north–south temperature gradient in the eastern part of Eurasia. The JJA precipitation change in the PM represents a triple structure with a substantial increase in precipitation over China and Korea (Figure 4(f)). The PM predicts a larger increase in JJA precipitation in the low latitudes to the south of 25°N, where relatively large range-to-mean ratios are evident (as shown in Figure 1(d)), while both GM and PM ensemble means suggest an increase in JJA precipitation over the East Asian monsoon region.

4.4. Results from the SNR

To evaluate model performance from a different statistical viewpoint, we apply the SNR to the 20C3M simulations for the period 1950–1999. The SNR is, in general, adequate for temperature and atmospheric moisture content, whereas precipitation and sea level pressure have a low SNR (Barnett and Schlesinger, 1987; Santer *et al*., 1991). Hence, only JFM 925-hPa temperature is analysed with the SNR. Figure 5(a) depicts a scatter diagram comparing SNR for East Asia with global SNR calculated from the 21 CGCMs. It is of interest that there is a linear relationship when the SNR is higher over both East Asia and globally. Over East Asia, a higher SNR is found in coastal regions, such as the east coast of China, the south coast of Korea, and around Japan (not shown). From the SNR scatter plot, the GM (PM) for the SNR is grouped with a threshold value of 0.5 (0.3) over East Asia and 1.3

Table II. The standard deviation and correlation coefficients between 21 IPCC AR4 CGCM simulation and observations for JFM 925-hPa air temperature over East Asia (100°E–150°E, 20°N–45°N).[a]

Model	Standard deviation	Correlation
CGCM3.1(T63)	**1.01**	**0.97**
CGCM3.1(T47)	**1.03**	**0.98**
CNRM-CM3	**1.06**	**0.98**
CSIRO-MK3.0	**1.03**	**0.99**
CSIRO-MK3.5	1.14	0.98
GFDL-CM2.0	1.12	0.95
GFDL-CM2.1	**0.98**	**0.99**
GISS-AOM	0.88	0.97
GISS-EH	1.03	0.96
GISS-ER	1.00	0.95
IAP-FGOALS1.0	1.04	0.96
IPSL-CM4	1.08	0.98
MIROC3.2(hires)	**1.06**	**0.98**
MIROC3.2(medres)	0.91	0.96
INMCM3.0	1.10	0.98
ECHAM5/MPI-OM	**0.97**	**0.99**
MRI-CGCM2.3.2	1.04	0.96
NCAR-CCSM3.0	1.05	0.97
NCAR-PCM1	1.10	0.97
ukMO-HadCM3	**1.03**	**0.97**
ukMO-HadGEM1	1.14	0.98

[a]The entries in bold represent the good performance models and their values.

Table III. The standard deviation and correlation coefficients between 21 IPCC AR4 CGCM simulations and observations for JJA precipitation over East Asia (100°E–150°E, 20°N–45°N).[a]

Model	Standard deviation	Correlation
CGCM3.1(T63)	**0.97**	**0.86**
CGCM3.1(T47)	0.92	0.68
CNRM-CM3	**0.98**	**0.91**
CSIRO-MK3.0	**1.09**	**0.86**
CSIRO-MK3.5	1.28	0.84
GFDL-CM2.0	**0.89**	**0.84**
GFDL-CM2.1	0.96	0.77
GISS-AOM	1.10	0.65
GISS-EH	1.01	0.81
GISS-ER	1.41	0.63
IAP-FGOALS1.0	1.13	0.79
IPSL-CM4	1.07	0.72
MIROC3.2(hires)	**1.17**	**0.84**
MIROC3.2(medres)	0.94	0.73
INMCM3.0	1.01	0.73
ECHAM5/MPI-OM	**1.12**	**0.86**
MRI-CGCM2.3.2	**1.17**	**0.85**
NCAR-CCSM3.0	1.12	0.81
NCAR-PCM1	0.97	0.61
ukMO-HadCM3	1.34	0.78
ukMO-HadGEM1	**1.11**	**0.85**

[a]The entries in bold represent the good performance models and their values.

(0.7) over the globe. The resultant grouping is indicated in the boxes inserted in Figure 5(a) and the corresponding models are listed in Table IV.

The GM ensemble mean change in JFM 925-hPa temperature indicates a prominent warming over central China compared to that indicated by the PM ensemble mean change (Figure 5(b)); this agrees well with the results obtained from the Taylor diagram (Figure 4(a)), although the spatial pattern and magnitude of the temperature are quite different. The GM also predicts the strengthening of the northwest–southeast temperature gradient across the south and southeast China margin. However, the ensemble mean of the PM shows a strong north–south temperature contrast around Korea and Japan and a weak warming over China (Figure 5(c)), which also agrees well with the results of the PM for the Taylor diagram (Figure 4(b)).

4.5. Results from principal-mode comparison

The ability of a climate model to capture interannual variability realistically is an important measure of its performance. To date, however, a faithful simulation of yearly rainfall over Asian monsoon regions has been a thorny issue for current CGCMs (e.g. Slingo *et al*., 1996; Kang *et al*., 2002). Thus, we only evaluate JFM 925-hPa temperature variability on a year-to-year timescale revealed as the first leading EOF mode. Figure 6(a) shows a scatter diagram between the EOF1 spatial correlation and PC1 temporal correlation. The simulated EOF1s explain about 30–40% of total variance over East Asia, which is comparable to the observed values. The models that reproduce the observed PC1 better tend to exhibit better performance in reproducing the observed EOF1. However, a GM for East Asia is not necessarily a GM for the entire globe (not shown). We select the GM for the EOF analysis as the models for which the correlation coefficients for both EOF1 and PC1 are significant at the 99% confidence level or higher (i.e. the models in the first quadrant in Figure 6(a)), and the PM as the models in the fourth quadrant in Figure 6(a). The selected models are listed in Table IV.

For the principal-mode approach, the projected temperature changes in the GM and PM are contrary to those predicted by the other statistical methods. The spatial changes of the EOF PM are akin to the GM changes of the Taylor diagram. It is noteworthy that four of the five models in the SNR GM belong to the EOF GM, which also predicts the northwest–southeast temperature contrast between the land and the ocean over East Asia and the warming in central China.

The ensemble means of JFM 925-hPa temperature and JJA precipitation from the GMs and the PMs for the SNR and the Taylor diagram are shown in Figure 7. The GM is composed of nine models (CGCM3.1(T63) overlap) and the PM of ten models, as shown in Table IV. It is noteworthy that four of the five models with good performance in terms of SNR belong to the GM for the EOF analysis. Therefore, the ensemble mean of the GM for the first two approaches is very similar to that for all three approaches. However, there is a slight difference in the ensemble mean of the PM between the first two approaches and the EOF analysis. The spatial pattern of

Table IV. Selected models for the good and poor groups based on each assessment methods; SNR, EOF, and Taylor diagram.

	Taylor diagram	SNR	EOF
Good group	CGCM3.1(T63)	CGCM3.1(T63)	CGCM3.1(T63)
	CNRM-CM3	GISS-AOM	GISS-AOM
	CSIRO-MK3.0	IPSL-CM4	IPSL-CM4
	MIROC3.2(hires)	MRI-CGCM2.3.2	GISS-ER
	ECHAM5/MPI-OH	ukMO-HadGEM1	ukMO-HadGEM1
Poor group	IPSL-CM4	CNRM-CM3	CSIRO-MK3.0
	NCAR-PCM1	GFDL-CM2.0	GFDL-CM2.0
	CSIRO-MK3.5	NCAR-CCSM3.0	GFDL-CM2.1
	GISS-ER	IAP-FGOALS1.0	NCAR-CCSM3.0
	INMCM3.0	MIROC3.2(medres)	ECHAM5/MPI-OH

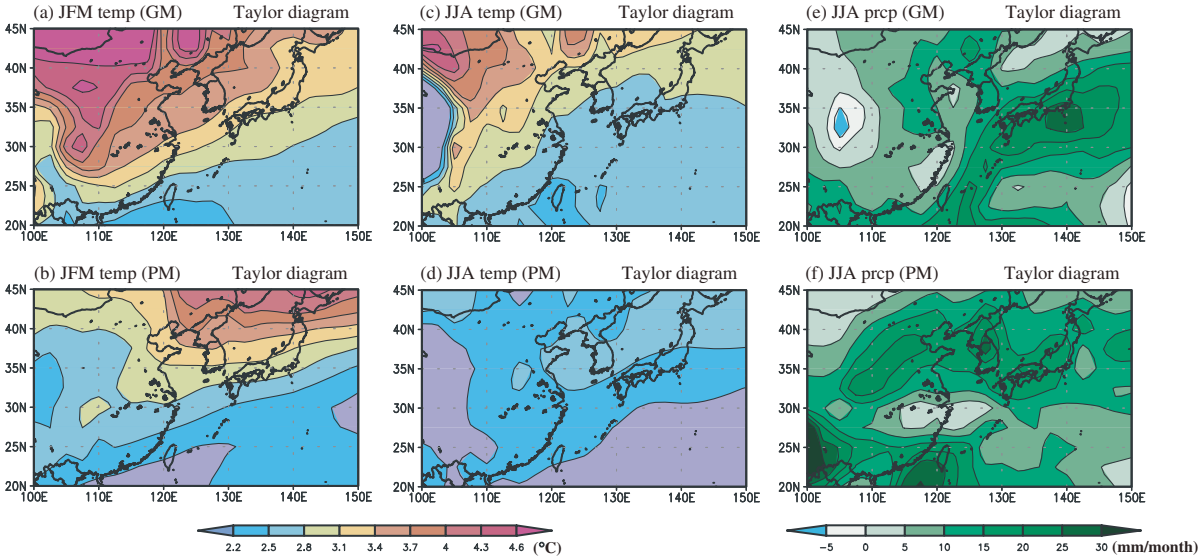

Figure 4. The change in JFM 925-hPa temperature (future minus present) over East Asia (100°E–150°E, 20°N–45°N) projected in (a) the good model group and (b) the poor model group for the Taylor diagram. (c) and (d) are the same as (a) and (b), respectively, but for JJA temperature. (e) and (f) are the same as (a) and (b), respectively, but for JJA precipitation. This figure is available in colour online at wileyonlinelibrary.com/journal/joc

the ensemble mean of the PM for the EOF is similar to that of the GM for the Taylor diagram and predicts higher warming over land than over ocean.

4.6. Results based on El Niño characteristics

Climatic anomalies in the western North Pacific and East Asia are related to the ENSO through tropical–extratropical and monsoon–ENSO interactions (Wang *et al*., 2000; Wang and Zhang, 2002; Yun *et al*. 2010a, 2010b). To investigate the remote coupling of changes in El Niño characteristics with projected changes in East Asian climate, Figure 8 presents a scatter plot relating East Asian climate change to the mean state change in the tropical Pacific (10°S–10°N, 120°E–80°W). The SST mean state change is defined as a spatial correlation between the SST EOF1 in the 20C3M simulations and a linear SST trend in the SRESA1B simulations as indicated in Section 3.4. Since the dominant mode of tropical SST variability delineates an El Niño-like oscillation in the CGCMs, a positive correlation indicates an El Niño-like warming in a future warmer climate. Prior to conducting the calculations, however, the reality of El Niño simulation was examined and three models (CSIRO-Mk3.0, GISS-AOM, and GISS Model E-R) were excluded as a result; in these models, the pattern correlation of the simulated EOF1 with its observed counterpart is lower than 0.5 for the region 30°S–30°N and 120°E–60°W. Figure 8 shows that most of the CGCMs simulate an El Niño-like warming, that is, SST warms more in the central and eastern equatorial Pacific than in the western equatorial and off-equatorial Pacific.

Interestingly, JFM 925-hPa temperature over East Asia varies as an inverse function of the change in the tropical Pacific mean state, with a correlation coefficient of −0.51 that is statistically significant at the 95% confidence level (Figure 8(a)). Conversely, there seems to be no reciprocity between the changes in the tropical Pacific mean state and East Asian summer precipitation (Figure 8(b)). However, it should be mentioned that a positive linear relationship with a correlation coefficient of 0.43 at the 90% confidence level can be seen when two

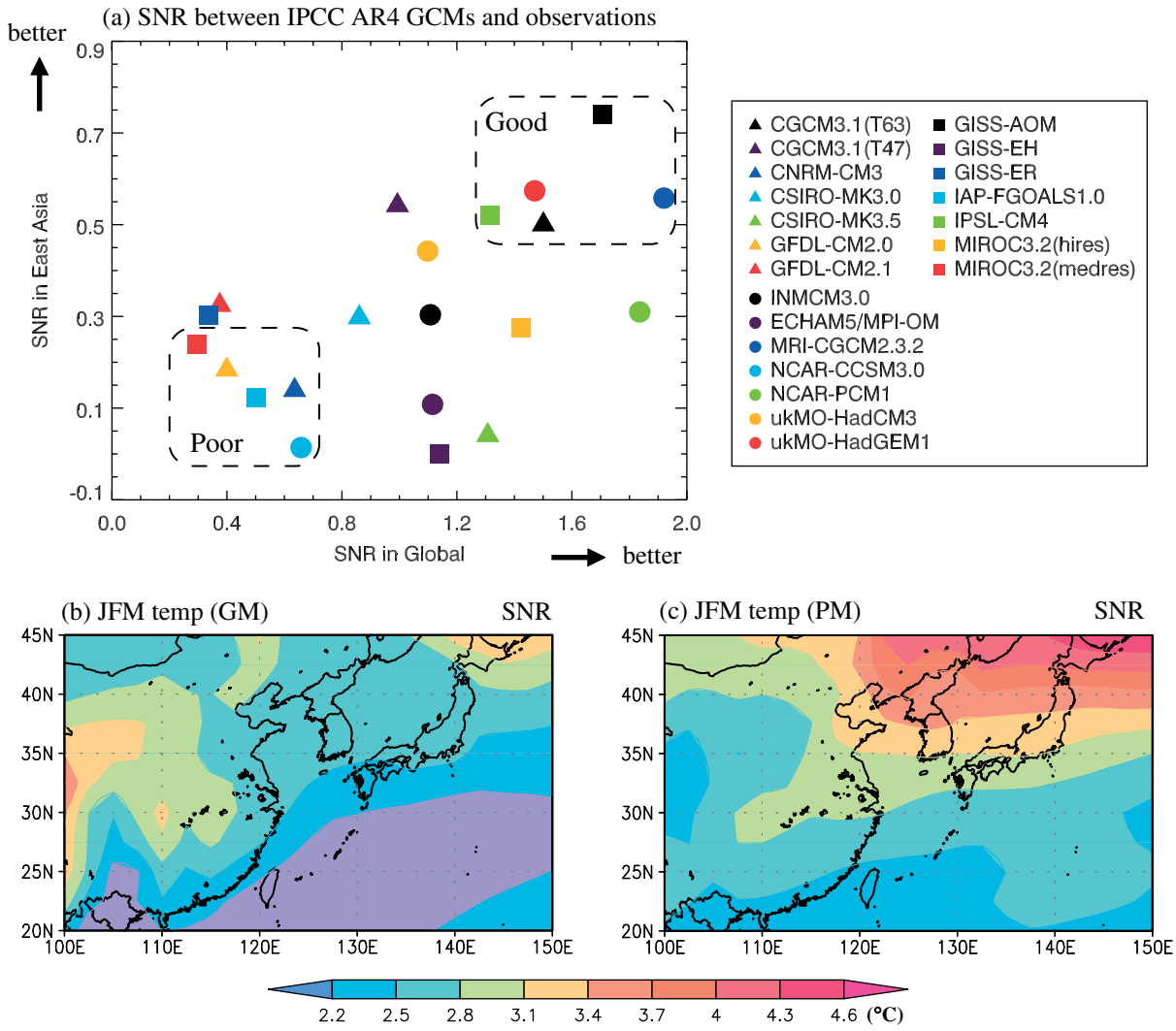

Figure 5. (a) Scatter diagram of signal-to-noise ratio (SNR) between simulated and observed JFM surface air temperature over East Asia (100°E–150°E, 20°N–45°N) *versus* over the globe. (b) and (c) depict the ensemble mean of the change in JFM 925-hPa temperature (future minus present) for the good model group and the poor model group, respectively. This figure is available in colour online at wileyonlinelibrary.com/journal/joc

outliers (CNRM-CM3 and GFDL-CM2.0) are ruled out. The results suggest that changes in winter temperature and summer precipitation over East Asia are sensitive to changes in the tropical Pacific mean state in the future climate.

5. Summary and discussion

This study aims to examine and predict the future climate over East Asia with greater confidence. To determine which models are most effective in projecting future regional climate, focusing on East Asia and Korea, we perform an uncertainty assessment of the 20C3M simulations from 21 IPCC AR4 CGCMs over a period covering 50 years from 1950 to 1999. The future climate changes are derived from the difference between the 20C3M simulations and the SRESA1B simulations for 2050–2099. First, we conjecture that climate models that can better simulate the present climate should be considered to be more dependable in projecting the future climate. The regional structures of climatological mean temperature and precipitation simulated by 21 CGCMs differ substantially from each other. Therefore, to ensure a credible prediction of regional climate change over East Asia, it is important to choose the CGCMs that have less uncertainty over the region.

We evaluate model performance in simulating JFM 925-hPa temperature and JJA precipitation over East Asia using the Taylor diagram, the SNR, and a principal-mode comparison. A comparison of the simulated present climate with the NCEP-1 dataset is conducted, alongside an analysis of the interannual variability of the present climate. In the uncertainty assessment using the Taylor diagram, the GM is composed of the best performance models for the variables. The GM for the Taylor diagram tends to predict larger warming over East Asia, particularly over land, as indicated by the enhancement of the northwest–southeast temperature gradient between

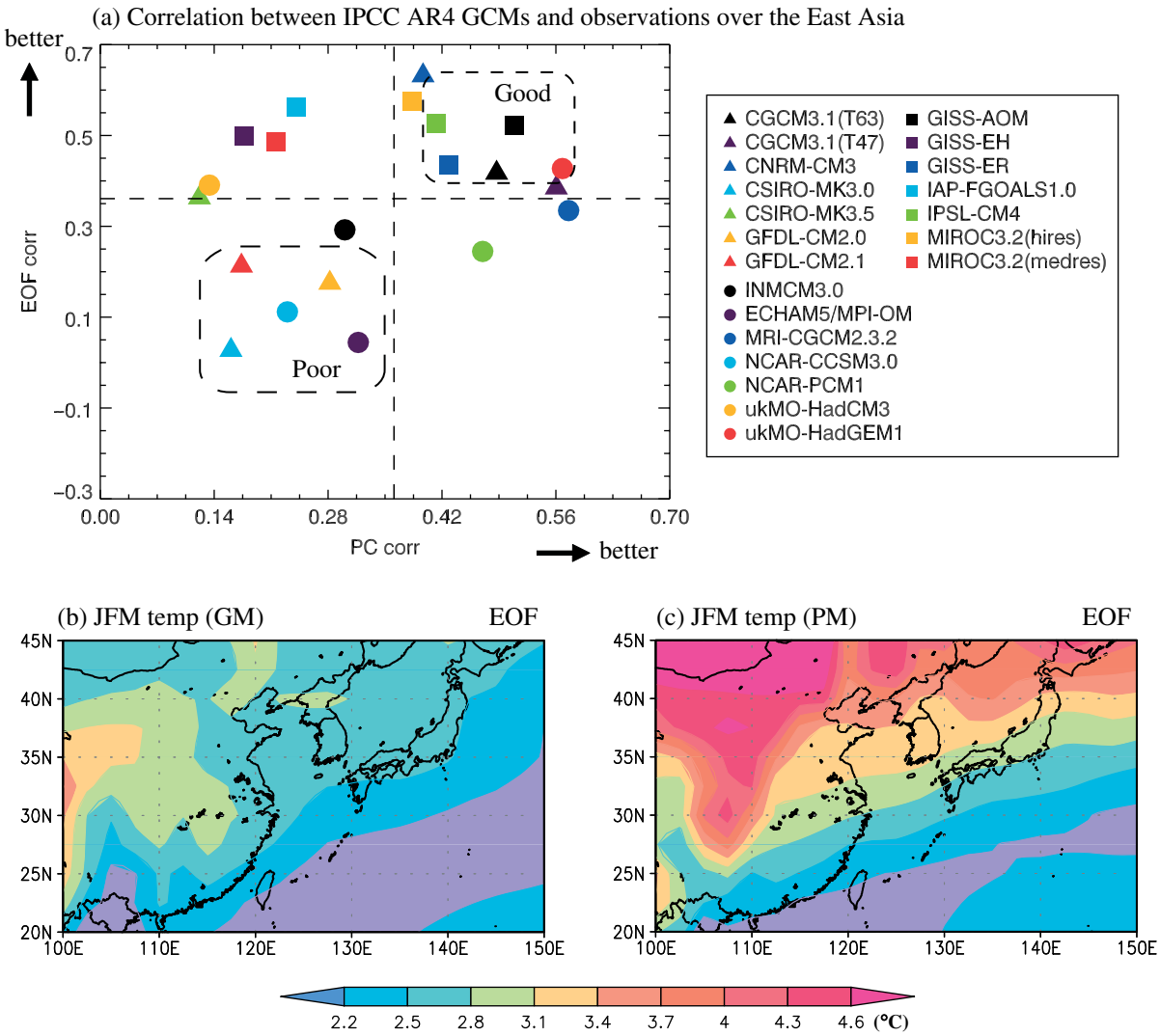

Figure 6. (a) A scatter diagram for pattern correlation of EOF1 *versus* correlation of PC1 between simulated and observed annual mean surface air temperature over East Asia (100°E–150°E, 20°N–45°N). (b) and (c) depict the ensemble mean of the change in JFM 925-hPa temperature (future minus present) for the good model group and the poor model group, respectively. The dashed line in (a) represents the 95% confidence level. This figure is available in colour online at wileyonlinelibrary.com/journal/joc

the land and ocean. This enhancement of the temperature gradient may strengthen anomalous ascending and descending motions over land and ocean with the EASM flow, which transports moisture from the East China Sea to Korea and Japan, resulting in greater increases in precipitation over the Baiu, Changma, and Meiyu bands. The GM for the SNR is determined by good performance models for both East Asia and the entire globe. The GM in the SNR predicts well the northwest–southeast temperature gradient and the warming over mid-China corresponding to that temperature gradient and warming over mid-China is also indicated by the Taylor diagram, although the spatial pattern and magnitude of the temperature are quite different. Principal-mode comparison indicates that the change in JFM air temperature is less for the GM than for the PM. However, the GM predicts well the northwest–southeast temperature gradient between the land and ocean over East Asia and the warming over mid-China.

We assess model performance based on El Niño characteristics, in addition to the three uncertainty assessment methods. For the mean state change in tropical Pacific SSTs, the CGCMs predicted that the El Niño-like warming would produce less warming in JFM over East Asia. This is consistent with the results from the principal-mode comparison, which are distinct from those of the Taylor and SNR approaches. This suggests that models that perform well in terms of the principal mode of climate variability tend to simulate more El Niño-like patterns and less East Asian warming. In this study, however, we do not examine a possible link between the change in the East Asian climate and that in the tropical Pacific mean state. The combination of the GM with the Taylor diagram and SNR suggests that future changes in global warming will be closer to the highest projected estimates; conversely, the models with good performance in terms of principal mode and tropical SST indicate that changes will be minor.

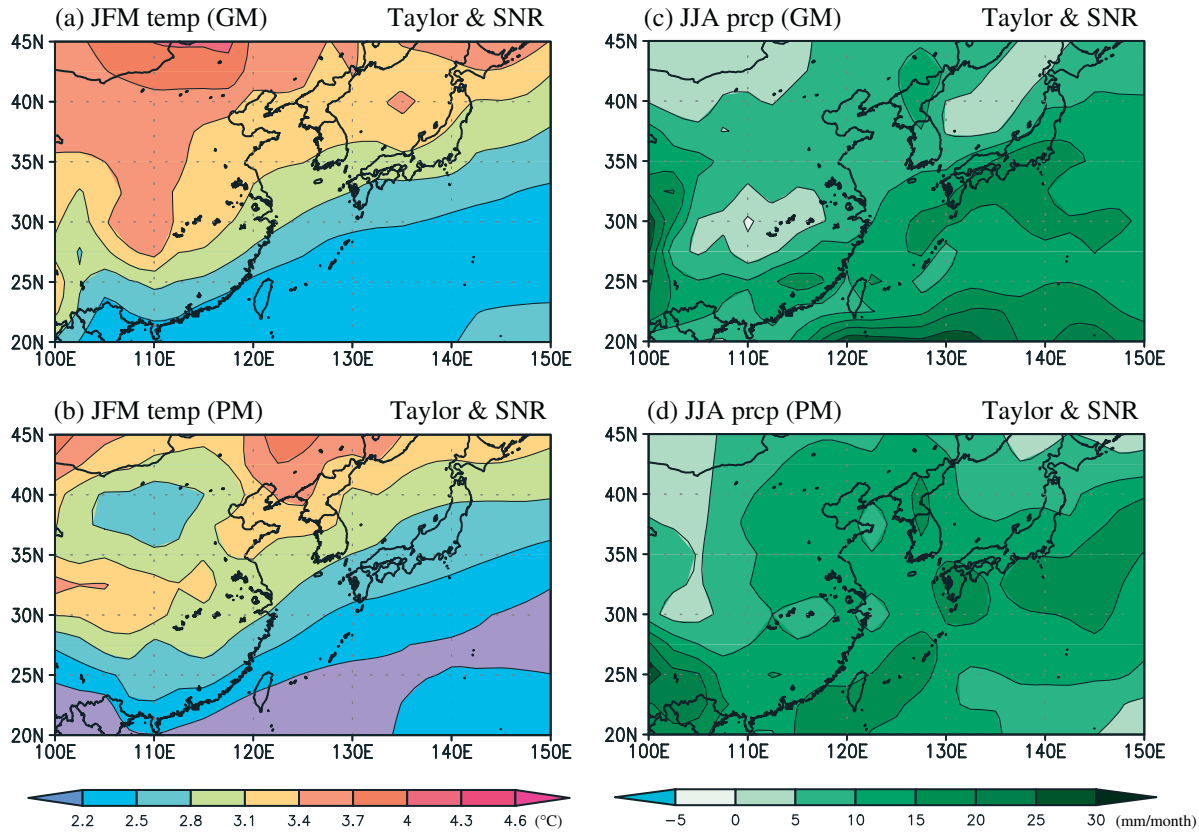

Figure 7. The change in JFM 925-hPa temperature over East Asia (100°E–150°E, 20°N–45°N) projected in (a) the good model group and (b) the poor model group for the combined method of the Taylor diagram and the SNR. (c) and (d) are the same as (a) and (b), respectively, but for JJA precipitation. This figure is available in colour online at wileyonlinelibrary.com/journal/joc

Because the reproduction of climate variability depends on the choice of CGCM, and because the variables considered important in assessing uncertainty depend on the assessment approach, the GM and PM selected vary according to assessment method. Although we evaluate model performance using the uncertainty assessment methods for regional climate prediction over East Asia, we have not yet been able to identify the best model for predicting climate change over this region. The answer will almost certainly depend on the intended application, since an accurate simulation of one aspect of climate does not guarantee an accurate representation of other aspects. An important implication of the present intermodel comparison, including uncertainty assessment and predictions from climate models on a regional scale, is that a good performance model must be chosen for regional climate prediction using the uncertainty assessment methods based on the dynamical or statistical viewpoint and the intended purpose. Furthermore, the choice of GMs with different weights according to the uncertainty assessment methods is very important to predict reliable future climate change.

Acknowledgements

This work was supported by GRL grant of the National Research Foundation (NRF) funded by the Korean Government (MEST 2011–0021927). We acknowledge the Korean Ministry of Environment for providing the output of the Eco-Technopia 21 Project. This study was conducted while the first author was a research professor at Pusan National University.

Appendix

A1 Relative entropy

Following Kleeman (2002) and Delsole and Tippett (2007), under the assumption of Gaussian distributions, the relative entropy between observation and model output can be defined by

$$R = \left[\log\frac{\sigma_a^2}{\sigma_f^2} + \frac{\sigma_f^2}{\sigma_a^2} - 1\right] + \left[\frac{(\mu_f - \mu_a)^2}{\sigma_a^2}\right] \qquad \text{(A1)}$$

where μ and σ are mean and variance, respectively, and subscripts a and f indicate observation and model prediction, respectively. The first two terms on the right hand side (RHS) of Equation (A1) are determined by the climatological variance and prediction variance, and represent the contribution of the dispersion or spread of the ensemble to relative entropy. The third term on the RHS of Equation (A1) is governed by the amplitude of the predicted ensemble mean and measures the contribution of the predicted signal size to relative entropy. The set of terms in the first bracket on the RHS is referred

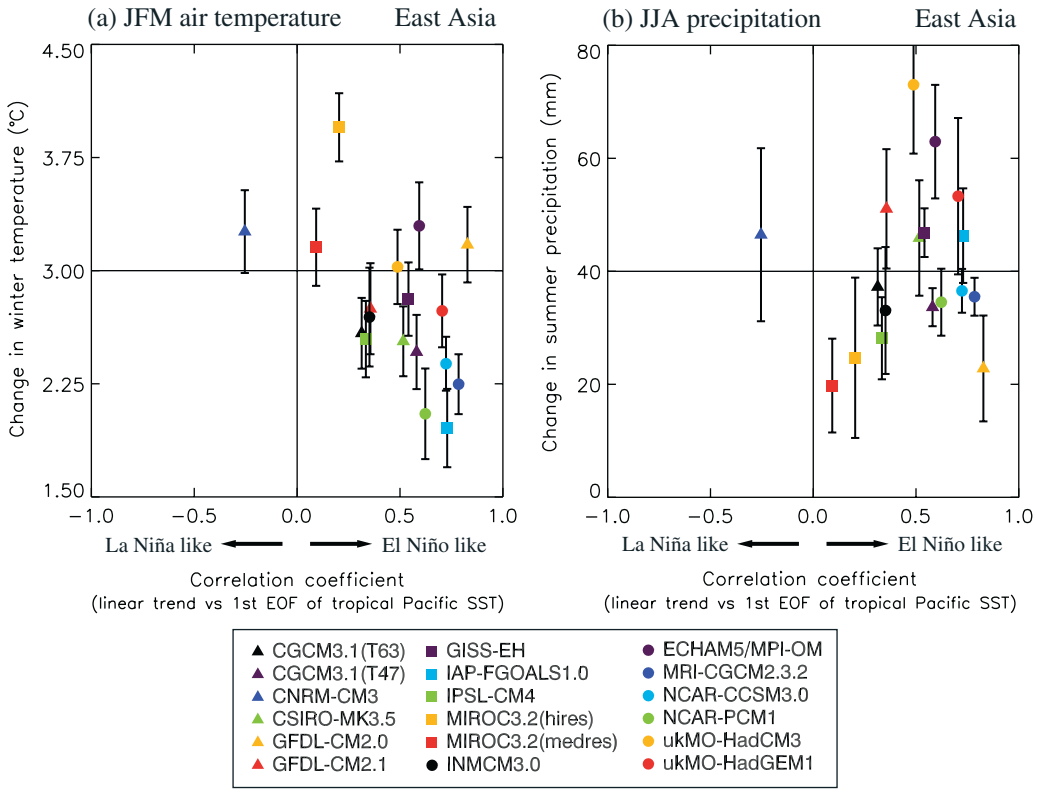

Figure 8. A scatter plot showing the change in the tropical Pacific mean state *versus* the change in (a) JFM 925-hPa temperature and (b) JJA precipitation over East Asia (100°E–150°E, 20°N–45°N). This figure is available in colour online at wileyonlinelibrary.com/journal/joc

to as the dispersion component and the second set as the signal component. The first term in the dispersion component indicates predictive information, while the second denotes the ratio of variance. The dispersion component measures the reduction in uncertainty of the random variables resulting from the prediction process. The signal is governed by the amplitude of the predicted mean field, which measures the contribution of the predicted signal size. The signal component is large when the means of the two distributions are large relative to the equilibrium spread for a sufficient number of principal components of the equilibrium distribution. Larger relative entropy indicates that more useful information is supplied by the model prediction.

A2 Signal-to-noise ratio

Trenberth *et al*. (1992) estimated the uncertainty and the differences in the observational datasets of sea surface temperature (SST) by calculating the size of the climate signal as measured by the actual temperature variations *versus* the noise. Let us consider two given time series with zero mean:

$$x(t) = z(t) + \varepsilon(t)$$

$$y(t) = z(t) + e(t) \qquad \text{(A2)}$$

where $z(t)$ is ostensibly the same quantity; $\varepsilon(t)$ and $e(t)$ are the noises in the datasets $x(t)$ and $y(t)$, respectively. The signal $z(t)$ will be measured by its variance S. The respective noises $\varepsilon(t)$ and $e(t)$, which are assumed to be random, give rise to noise variances N_x and N_y. Thus, the correlation coefficient, r, between x and y is

$$r = \frac{S}{\sigma_x \sigma_y} \qquad \text{(A3)}$$

where σ is the standard deviation. Because $\sigma_x = S + N_x$ and $\sigma_y = S + N_y$, the average noise is

$$N = 0.5\left(N_x + N_y\right) = 0.5\left(\sigma_x^2 + \sigma_y^2 - 2r\sigma_x\sigma_y\right) \qquad \text{(A4)}$$

Using r, the signal-to-noise ratio (SNR) is

$$\frac{S}{N} = \frac{2r}{\left(\frac{\sigma_x}{\sigma_y} + \frac{\sigma_y}{\sigma_x} - 2r\right)} \qquad \text{(A5)}$$

and the correlation coefficient can be a measure of the SNR. In addition, if $\sigma_x \approx \sigma_y$, the SNR can be simplified as $(S/N) = (r/1 - r)$. The signal is always detectable when the true SNR is much larger than 1.

Some climate signals are captured by some models but not others. This suggests that, in addition to sampling the uncertainty arising from imperfect knowledge of initial conditions, the uncertainty arising from imperfect knowledge of the physical processes must also be sampled, specifically those represented through parameterizations.

References

Barnett TP, Schlesinger ME. 1987. Detecting changes in global 306 references climate induced by greenhouse gases. *Journal of Geophysical Research* **92**: 14772–14780.

Boer GJ, Lambert SJ. 2001. Second order space–time climate difference statistics. *Climate Dynamics* **17**: 213–218.

Bueh C, Cubasch U, Hagemann S. 2003. Impacts of global warming on changes in the East Asian monsoon and the related river discharge in a global time-slice experiment. *Climate Research* **24**: 47–57.

Collins WD, Bitz CM, Blackmon ML, Bonan GB, Bretherton CS, Carton, JA, Chang P, Doney SC, Hack JJ, Henderson TB, Kiehl JT, Large WG, McKenna DS, Santer BD, Smith RD. 2006. The community climate system model version 3 (CCSM3). *Journal of Climate* **19**: 2122–2143.

Cover TM, Thomas JA. 1991. *Elements of Information Theory*. John Wiley and Sons: New York.

Delsole T. 2004. Predictability and information theory. Part I: measures of predictability. *Journal of Atmospheric Sciences* **61**: 2425–2440.

Delsole T, Tippet MK. 2007. Predictability: recent insights from information theory. *Reviews of Geophysics* **45**: RG4002. DOI: 10.1029/2006RG000202.

Delworth TL, Broccoli AJ, Rosati A, Stouffer RJ, Balaji V, Beesley JA, Cooke WF, Dixon KW, Dunne J, Dunne KA, Durachta JW, Findell KL, Ginoux P, Gnanadesikan A, Gordon CT, Griffies SM, Gudgel R, Harrison MJ, Held IM, Hemler RS, Horowitz LW, Klein SA, Knutson TR, Kushner PJ, Langenhorst AR, Lee H-C, Lin S-S, Lu J, Malyshev SL, Milly PCD, Ramaswamy V, Russell J, Schwarzkopf MD, Shevliakova E, Sirutis JJ, Spelman MJ, Stern WF, Winton M, Wittenberg AT, Wyman B, Zeng F, Zhangc R. 2006. GFDLs CM2 global coupled climate models. Part I: formulation and simulation characteristics. *Journal of Climate* **19**: 643–674.

Diansky NA, Volodin EM. 2002. Simulation of present-day climate with a coupled Atmosphere–ocean general circulation model. *Atmospheric and Oceanic Physics* **38**: 732–747.

Giannakis D, Majda AJ. 2012. Quantifying the predictive skill in long-range forecasting. Part II: Model error in coarse-grained Markov models with application to ocean-circulation regimes. *Journal of Climate* **25**: 1814–1826.

Gleckler PJ, Taylor KE, Doutriaux C. 2008. Performance metrics for climate models. *Journal of Geophysical Research* **113**: D06104. DOI: 10.1029/2007JD008972.

Gordon HB, Rotstayn LD, McGregor JL, Dix MR, Kowalczyk EA, O'Farrel SP, Waterman LJ, Hirst AC, Wilson SG, Collier MA, Watterson IG, Elliott TI. 2002. *The CSIRO Mk3 climate system model*, Technical Paper No. 60, CSIRO Atmospheric Research, Aspendale, Victoria, Australia.

Gordon C, Cooper C, Senior CA, Banks H, Gregory JM, Johns TC, Mitchell JFB, Wood RA. 2000. The simulation of SST, sea ice extents and ocean heat transports in a version of the Hadley Centre coupled model without flux adjustments. *Climate Dynamics* **16**: 147–168.

Guilyardi E, Wittenberg A, Fedorov A, Collins M, Wang C, Capotondi A, van Oldenborgh GJ, Stockdale J. 2009. Understanding El Niño in ocean–atmosphere general circulation models: progress and challenges. *Bulletin of the American Meteorological Society* **90**: 325–340.

Ha K-J, Heo K-Y, Lee S-S, Yun K-S, Jhun J-G. 2012. Variability in the East Asian Monsoon: a review. *Meteorological Applications* **19**: 200–215.

Intergovernmental Panel on Climate Change. 2007. *Climate Change 2007: The Physical Science Basis*. Contribution of Working Group I to the Fourth Assessment Report of the Intergovernmental Panel on Climate Change, Solomon S, *et al.* (eds). 996 pp., Cambridge University Press: Cambridge.

Johns T, Durman C, Banks H, Roberts M, McLaren A, Ridley J, Senior C, Williams K, Jones A, Keen A, Rickard G, Cusack S, Joshi M, Ringer M, Dong B, Spencer H, Hill R, Gregory J, Pardaen A, Lowe J, Bodas-Salcedo A, Stark S, Searl Y. 2004. *HadGEM1–Model description and analysis of preliminary experiments for the IPCC Fourth Assessment Report*. Technical Report, 55, Met Office, Exeter.

Jungclaus JH, Keenlyside N, Botzet M, Haak H, Luo J-J, Latif M, Marotzke J, Mikolajewicz U, Roeckner E. 2006. Ocean circulation and tropical variability in the coupled model ECHAM5/MPI-OM. *Journal of Climate* **19**: 3952–3972.

K-1 model developers. 2004. *K-1 coupled model (MIROC) description. K-1 Technical Report 1*. Center for Climate System Research, University of Tokyo.

Kalnay E, Kanamitsu M, Kistler R, Collins W, Deaven E, Gandin L, Iredell M, Saha S, White G, Woollen J, Zhu Y, Leetmaa A, Reynolds R, Chelliah M, Ebisuzaki W, Higgins W, Janowiak J, Mo KC, Ropelewski C, Wang J, Jenne R, Joseph D. 1996. The NCEP/NCAR 40-Year reanalysis project. *Bulletin of the American Meteorological Society* **77**: 437–471.

Kang IS, Jin K, Wang B, Lau K-M, Shukla J, Krishnamurthy V, Schubert SD, Wailser DE, Stern WF, Kitoh A, Meehl GA, Kanamitsu M, Galin VY, Satyan V, Park C-K, Liu Y. 2002. Intercomparison of the climatological variations of Asian summer monsoon precipitation simulated by 10 GCMs. *Climate Dynamics* **19**: 383–395.

Kleeman R. 2002. Measuring dynamical prediction utility using relative entropy. *Journal of Atmospheric Sciences* **59**: 2057–2072.

Kullback S. 1959. *Information Theory and Statistics*. John Wiley and Sons: New York.

Labraga JC. 2005. Simulation capability of tropical and extratropical seasonal climate anomalies over South America. *Climate Dynamics* **25**: 427–445.

Lambert SJ, Boer GJ. 2001. CMIP1 evaluation and intercomparision of coupled climate models. *Climate Dynamics* **17**: 83–106.

Lucarini L, Russell GL. 2002. Comparison of mean climate trends in the northern hemisphere between National Centers for Environmental Prediction and two atmosphere–ocean model forced runs. *Journal of Geophysical Research* **107**: 4269. DOI: 10.1029/2001JD001247.

Marti O, Braconnot P, Bellier J, Benshila R, Bony S, Brockmann P, Cadule P, Caubel A, Denvil S, Dufresne JL, Fairhead L, Filiberti M-A, Fichefet T, Foujols M-A, Friedlingstein P, Grandpeix J-Y, Hourdin F, Krinner G, Levy C, Madec G, Musat I, De Noblet N, Polcher J, Talandier C. 2005. *The new IPSL climate system model: IPSL-CM4*. Technical Report, Institut Pierre Simon Laplace des Sciences de l''Environment Global, IPSL, Case 101, Paris.

McFarlane NA, Scinocca JF, Lazare M, Harvey R, Verseghy D, Li J. 2005. *The CCCma third generation atmospheric general circulation model*. CCCma Internal Report, 25 pp.

Mu Q, Jackson CS, Stoffa PL. 2004. A multivariate empirical-orthogonal-function-based measure of climate model performance. *Journal of Geophysical Research* **109**: D15101. DOI: 10.1029/2004JD004584.

Rayner NA, Parker DE, Horton EB, Folland CK, Alexander LV, Rowell DP, Kent EC, Kaplan A. 2003. Global analyses of sea surface temperature, sea ice, and night marine air temperature since the late nineteenth century. *Journal of Geophysical Research* **108**(D14): 4407. DOI: 10.1029/2002JD002670.

Reichler T, Kim J. 2008. How well do coupled models simulate today's climate? *Bulletin of the American Meteorological Society* **89**(3): 303–311.

Salas-Mélia D, Chauvin F, deque M, Douville H, Gueremy JF, Marquet P, Planton S, Royer JF, Tyteca S. 2005. *Description and validation of the CNRM–CM3 global coupled model*. CNRM Technical Report 103, 36 pp.

Santer BD, Wigley TML, Jones PD, Schlesinger ME. 1991. Multivariate methods for the detection of greenhouse-gas-induced climatic change. In *Greenhouse-Gas-Induced Climatic Change: A Critical Appraisal of Simulations and Observations*, Schlesinger ME (ed). Elsevier Science; 511–536.

Santer BD, Briigemann W, Cubasch U, Hasselmann K, Höck H, Maier-Reimer E, Mikolajewicz U. 1994. Signal-to-noise analysis of time-dependent greenhouse warming experiments. *Climate Dynamics* **9**: 267–285.

Schaller N, Mahlstein I, Cermak J, Knutti R. 2011. Analyzing precipitation projections: a comparison of different approaches to climate model evaluation. *Journal of Geophysical Research* **116**: D10118. DOI: 10.1029/2010JD014963.

Schmidt GA, Ruedy R, Hansen JE, Aleinov I, Bell N, Bauer M, Bauer S, Cairns B, Canuto V, Cheng Y, Del Genio A, Faluvegi G, Friend AD, Hall TM, Hu Y, Kelley M, Kiang NY, Koch D, Lacis AA, Lerner J, Lo KK, Miller RL, Nazarenko L, Oinas V, Perlwitz JP, Perlwitz J, Rind D, Romanou A, Russell GL, Sato M, Shindell DT, Stone PH, Sun S, Tausnev N, Thresher D, Yao M-S. 2006. Present-day atmospheric simulations using GISS Model E: comparison to in situ, satellite, and reanalysis data. *Journal of Climate* **19**: 153–192.

Scinocca JF, McFarlane NA, Lazare M, Li J, Plummer D. 2008. The CCCma third generation AGCM and its extension into the middle atmosphere. *Atmospheric Chemistry and Physics* **8**: 7055–7074.

Shukla J, DelSole T, Fennessy M, Kinter J, Paolino D. 2006. Climate model fidelity and projections of climate change. *Geophysical Research Letters* **33**: L07702. DOI: 10.1029/2005GL025579.

Slingo JM, Sperber KR, Boyle JS, Ceron JP, Dix M, Dugas B, Ebisuzaki W, Fyfe J, Gregory D, Gueremy JF, Hack J, Harzallah A, Inness P, Kitoh A, Lau WK-M, McAvaney B, Madden R, Matthews A, Palmer TN, Parkas C-K, Randall D, Renno N. 1996. Intraseasonal oscillations in 15 atmospheric general circulation models: results from an AMIP diagnostic subproject. *Climate Dynamics* **12**: 325–357.

Tang Y, Lin H, Moore AM. 2008. Measuring the potential predictability of ensemble climate predictions. *Journal of Geophysical Research* **113**: D04108. DOI: 10.1029/2007JD008804.

Taylor KE. 2001. Summarizing multiple aspects of model performance in a single diagram. *Journal of Geophysical Research* **106**: 7183–7192.

Tippett MK, Kleeman R, Tang Y. 2004. Measuring the potential utility of seasonal climate predictions. *Geophysical Research Letters* **31**: L22201. DOI: 10.1029/2004GL021575.

Trenberth KE, Christy JR, Hurrell JW. 1992. Monitoring global monthly mean surface temperatures. *Journal of Climate* **5**: 1405–1423.

Wang B, Wu R, Fu X. 2000. Pacific–East Asian teleconnection: how does ENSO affect East Asian climate? *Journal of Climate* **13**: 1517–1536.

Wang B, Zhang Q. 2002. Pacific–East Asian teleconnection. Part II: how the Philippine Sea anomalous anticyclone is established during El Niño development. *Journal of Climate* **15**: 3252–3265.

Washington WM *et al.* 2000. Parallel climate model (PCM) control and transient simulations. *Climate Dynamics* **16**: 755–774.

Xie P, Arkin PA. 1997. Global precipitation: a 17-year monthly analysis based on gauge observations, satellite estimates and numerical model outputs. *Bulletin of the American Meteorological Society* **78**: 2539–2558.

Yeh SW, Kirtman BP. 2006. The characteristics of signal versus noise SST variability in the North Pacific and the Tropical Pacific Ocean. *Ocean Science Journal* **41**(1): 1–10.

Yu Y, Zhang X, Guo Y. 2004. Global coupled ocean atmosphere general circulation models in LASG/IAP. *Advances in Atmospheric Sciences* **21**: 444–455.

Yukimoto S, Noda A. 2002. *Improvements of the Meteorological Research Institute Global Ocean–atmosphere Coupled GCM (MRI-CGCM2) and its climate sensitivity*. Technical Report 10, NIES, Japan, 8.

Yun K-S, Ha K-J, Wang B. 2010a. Impacts of tropical ocean warming on East Asian summer climate. *Geophysical Research Letters* **37**: L20809. DOI: 10.1029/2010GL044931.

Yun K-S, Seo K-H, Ha K-J. 2010b. Interdecadal change in the relationship between ENSO and the Intraseasonal Oscillation in East Asia. *Journal of Climate* **23**: 3599–3612.

Zwiers FW, von Storch H. 2004. On the role of statistics in climate research. *International Journal of Climatology* **24**: 665–680.

